Tunable electronic properties and enhanced ferromagnetism in Cr2Ge2Te6 monolayer by strain engineering

Liu, L.; Hu, X.; Wang, Y.; Krasheninnikov, A.; Chen, Z.; Sun, L.;

Originally published:

September 2021

Nanotechnology 32(2021), 485408

DOI: https://doi.org/10.1088/1361-6528/ac1a94

Tunable electronic properties and enhanced ferromagnetism in $Cr_2Ge_2Te_6$ monolayer by strain engineering

Lifei Liu,[1] Xiaohui Hu,[*1,2] Yifeng Wang,[1,2] Arkady V. Krasheninnikov,[3,4]

Zhongfang Chen,[5] Litao Sun[6]

[1] College of Materials Science and Engineering, Nanjing Tech University, Nanjing 211816, China

[2] Jiangsu Collaborative Innovation Center for Advanced Inorganic Function Composites, Nanjing Tech University, Nanjing 211816, China

[3] Institute of Ion Beam Physics and Materials Research, Helmholtz-Zentrum Dresden-Rossendorf, 01314 Dresden, Germany

[4] Department of Applied Physics, Aalto University School of Science, PO Box 11100, 00076 Aalto, Finland

[5] Department of Chemistry, University of Puerto Rico, Rio Piedras Campus, San Juan, Puerto Rico 00931

[6] SEU-FEI Nano-Pico Center, Key Laboratory of MEMS of Ministry of Education, Collaborative Innovation Center for Micro/Nano Fabrication, Device and System, Southeast University, Nanjing 210096, China

Corresponding Author: xiaohui.hu@njtech.edu.cn (X Hu)

Abstract

Recently, as a new representative of Heisenberg's two-dimensional (2D) ferromagnetic materials, 2D $Cr_2Ge_2Te_6$ (CGT) has attracted much attention due to its intrinsic ferromagnetism. Unfortunately, the Curie temperature (T_C) of CGT monolayer is only 22K, which greatly hampers the development of the applications based on the CGT materials. Herein, the electronic and magnetic properties of $Cr_2Ge_2Te_6$ monolayer under the applied strain was explored by density functional theory calculation. It is demonstrated that the band gap of CGT monolayer can be remarkably modulated by applying the tensile strain, which first increases and then decreases with the increase of tensile strain. In addition, it is found that the strain can increase the Curie temperature and magnetic moment, so that largely enhance the ferromagnetism of CGT monolayer. Notably, the obvious enhancement of T_C by 191% is achieved at 10% strain. The results demonstrate that strain engineering can not only tune the electronic properties, but also provide a promising avenue to improve the ferromagnetism of CGT monolayer. The remarkable electronic and magnetic response to biaxial strain can also facilitate the development of CGT-based spin devices.

Keywords: Density functional theory, $Cr_2Ge_2Te_6$, Electronic properties, Magnetic properties, Curie temperature, Strain engineering

Introduction

The research on two-dimensional (2D) materials has rapidly been progressing due to their rich physico-chemical properties [1-9]. However, many 2D materials such as graphene, black phosphorus, and h-BN, etc., have no magnetism, which limits their

applications in spintronics. To add this functionality to nonmagnetic 2D materials, many approaches such as introduction of defects [10-11], doping [12-14] and adsorption of atoms and molecules [15-16]. Unfortunately, the coupling of magnetic moments induced by these methods in otherwise nonmagnetic 2D materials was local or strongly dependent on the environment. Therefore, attention has been focused on the search for new intrinsically magnetic 2D materials. Encouragingly, some 2D ferromagnetic materials such as $Cr_2Ge_2Te_6$, CrI_3 and Fe_3GeTe_2 have been successfully synthesized [17-20]. The existence of the long-range ferromagnetic order in them can overcome the limitations mentioned above.

Recently, experiments have confirmed the intrinsic magnetism in 2D CrI_3, $Cr_2Ge_2Te_6$ and Fe_3GeTe_2. It is a promising research goal to identify 2D semiconductors with room temperature ferromagnetic order. The Fe_3GeTe_2 monolayer has a Curie temperature of 130K, but exhibits metallic character [21], while magnetic semiconducting materials are required for spintronics. The CrI_3 monolayer has been reported as a new type of Ising ferromagnet with out-of-plane spin orientation [17]. Almost at the same time, another intrinsic ferromagnetic semiconductor $Cr_2Ge_2Te_6$ bilayer has been successfully prepared in experiments [18]. As a promising Heisenberg's 2D ferromagnetic with strong magnetic anisotropy energy and magneto-optical effects, $Cr_2Ge_2Te_6$ has potential application in spintronic nanodevices [22-24]. Xu et al. predicted that magnetic anisotropy of $Cr_2Ge_2Te_6$ monolayer was mainly single ion anisotropy [26]. However, the Curie temperature in $Cr_2Ge_2Te_6$ is only 22K [18], which greatly hampers the development of $Cr_2Ge_2Te_6$ materials for spintronic devices. Accordingly, it is very

important to enhance ferromagnetic stability $Cr_2Ge_2Te_6$ and modulate the magnetic moment [27-28]. For example, it was predicted that the electromagnetic properties of CGT monolayer significant change upon adsorption of gas molecules. In particular, NO adsorption increased the Curie temperature by 38% [27]. The magnetic anisotropy energy and Curie temperature can be increased, correspondingly, by a factor of four and 33%, as compared to the pristine $Cr_2Ge_2Te_6$ by H and alkali-metal adsorption [28]. In addition, Ge vacancies remarkably enhance the magnetic anisotropy energy of $Cr_2Ge_2Te_6$ monolayer [29].

Strain engineering is proposed as one of the most commonly used routes to tailor the electronic and magnetic properties of 2D materials [30-40]. In our previous study, we demonstrated that the band gap of zigzag BCN hybrid materials with zigzag arrangement of graphene and h-BN stripes decreases under biaxial tensile strain, while the band gap of armchair BCNs material varies more complicated with strain and related to C concentration [30]. The band structure of TMDs can be continuously tuned by applying the uniaxial and biaxial tensile strains [31]. The transition from the direct to the indirect band gap can be achieved under the uniaxial compression and tensile strains in black phosphorus [32]. The transition from ferromagnetic to antiferromagnetic state under compressive strain was predicted for CrX_3 (X = Cl, Br, I) [33]. External strain can considerably enhance the stability and tune the magnetic moments of the CoB_6 monomolecular layer [34]. It is proposed that because the VX_2 (X = S, Se) monolayer has strong ionic covalent bonds, the tensile strain can remarkably increase its magnetic moment [36]. Therefore, it is very necessary to investigate the

strain dependence on the electronic and magnetic properties of $Cr_2Ge_2Te_6$.

In this work, we study the electronic and magnetic properties of CGT monolayer under a biaxial tensile strain by means of systematic density functional theory calculations. The results show that the tensile strain can not only effectively tune the band gap of CGT monolayer, but also significantly enhance the ferromagnetism. The Curie temperature increases by 191% under 10% tensile strain. As the strain applied increases, the magnetic moment of Cr atom increases monotonically. Our results suggest that strain engineering can effectively tune the band gap and enhance the ferromagnetic properties of CGT monolayers, which provides a new way to design spin devices based on CGT.

Computational methods

Our calculations are carried out within the framework of the DFT using the Vienna ab initio Simulation Package (VASP) [41, 42] and the projector-augmented-wave (PAW) method [43, 44]. In the generalized gradient approximation (GGA), the Perdew-Burke-Ernzerhof (PBE) [45] functional is used to describe the exchange and correlations. In Brillouin zone, 9 × 9 × 1 k-point grid mesh sampling was used, and a vacuum thickness was introduced along the z-axis at least 15Å to avoid any artificial interactions between periodic images of slabs. The plane-wave cutoff energy was set to 500 eV. The lattice constants and atom coordinates are optimized with the energy convergence value is set as 1×10^{-6} eV and the force is set as 0.005 eV/Å. PBE + U functional is used to examine the lattice constants and magnetic moment of CGT monolayer. The Hubbard U value of Cr atom is set to 2.0 eV [28]. In addition, the electronic structure of CGT monolayer

is studied by the hybrid function HSE06 [46].

Results and discussion

Recently, few- and double-layer CGT ferromagnetic materials have been successfully synthesized by Zhang and co-workers in 2017 [18]. Experimental results revealed that ultrathin layered CGT is ferromagnetic at low temperatures. The Cr atoms in CGT monolayer form a 2D honeycomb spin arrangement, while the hexagonal region between them is occupied by Ge dimer and Te octahedron with shared edges, as shown in figure 1(a). The optimized lattice constants of CGT monolayer are a = b = 6.91 Å, which is consistent with the previous theoretical research results [22, 28]. The nearest-neighbor bond length $d_{Cr\text{-}Te}$ is 2.78 Å, which also agrees well with the previous reports [27]. In order to obtain the ground state of CGT monolayer, ferromagnetic (FM), Néel antiferromagnetic (Néel-AFM), stripy-AFM and zigzag-AFM magnetic configurations are considered (igure S1, Supporting Information). It is found that FM configuration is more stable than the AFM ones. Among the three AFM configurations, the Néel-AFM configuration is the energetically more favorable than stripy-AFM and zigzag-AFM ones. The spin density distribution reveals that the magnetic moment of CGT monolayer is mainly localized on Cr atom (see figure 1(b)), and the magnetic moment per Cr atom is 3.17μ_B. As can be seen from the band structure (Figure 1(c)), CGT monolayer is an indirect semiconductor with the band gap of 0.37eV, well consistent with previously reported results [47]. The conduction band minimum (CBM) and valence band maximum (VBM) are located at K and Γ points, respectively. Moreover, the projected density of states (PDOS) indicates that the CBM and VBM are mainly

localized at the *d* orbitals of Cr atoms and the *p* orbitals of Te atoms respectively, as evident from figure 1(d). The lattice constant and magnetic moment of CGT monolayer were also examined by the PBE+U method, shown in Table S1 of Supporting Information. It is found that the lattice constant and magnetic moment remain unchanged. We also calculated the band structure of CGT monolayer based on the hybrid HSE06 functional. As shown in figure S2 of Supporting Information, the band gap of CGT monolayer can be obviously increased.

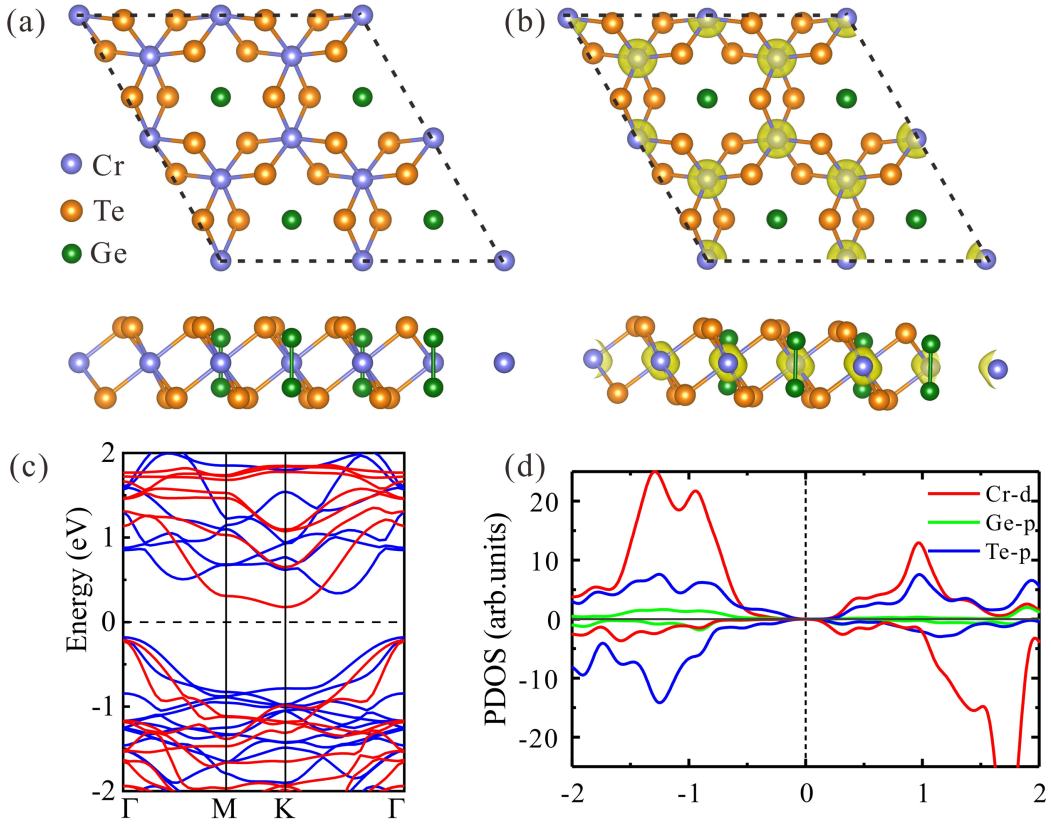

Figure 1. (a) Top and side views of the optimized geometries of the $Cr_2Ge_2Te_6$ monolayer. (b) Spin density distribution and (c) band structure of the CGT monolayer, the red and blue lines represent spin-down and spin-up channels, respectively. (d) The PDOS of the pristine CGT monolayer. The Fermi level is set at zero.

The strain dependence of the electronic and magnetic properties of the CGT monolayer was investigated by varying the biaxial tensile strain without changing honeycomb-like structures and crystal symmetries. The biaxial tensile strain is defined as $\varepsilon = \Delta c/c_0$, where c_0 and $c_0 \pm \Delta c$ are the lattice constants of the unstrained and strained CGT monolayer, respectively. Δc is the displacement along the lattice coordinates [30]. In order to assess the stability of CGT monolayer under strain, CGT monolayer under 10% strain was selected for further stability evaluation. We performed molecular dynamics (MD) simulations based on the DFT in a canonical ensemble of temperatures and times of 300K and 5ps respectively [13, 30]. As seen from figure 2(a), the CGT structure was not disrupted at room temperature during the simulation time. Although the simulation time is not macroscopic, this result can be considered as evidence for the stability of the system. Taking this into account, we studied the electronic and magnetic properties of CGT monolayer at the strain varies from 0% to 10%.

We show the variation of band gap of CGT monolayer with applied strain in figure 2(b). As a result, different from the band gap decrease in CrI_3, graphene and h-BN with the increasing tensile strain [33, 48], it is obvious that the band gap of CGT monolayer first increases and then decreases as tensile strain increases. Specifically, the band gap of CGT monolayer increases from 0.37 eV to 0.71 eV with tensile strain from 0% to 4%, and then decreases to 0.38 eV at 10% strain.

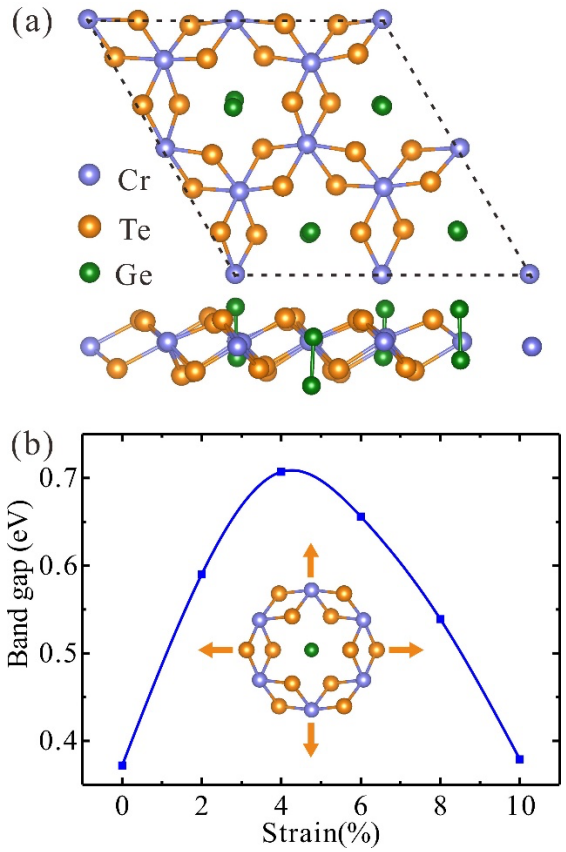

Figure 2. (a) Top and side views of the snapshots of CGT monolayer taken after 5 ps of DFT-MD simulations at 300 K, (b) strain effect on the band gap of CGT monolayer. The inset schematically shows strain directions.

The band structures of CGT monolayer under 0 to 10% biaxial strains are presented in figure 3(a-c) and figure S3. The CGT monolayer exhibits an indirect band gap with 0.37 eV, 0.71 eV and 0.54 eV under 0%, 4% and 8% strains, respectively. One can clearly see that the lowest conduction band (LCB) and the highest valence band (HVB) simultaneously move away the Fermi level as strain values from 0% to 4%, which increases the band gap of CGT monolayer to 0.71 eV. In contrast, as the strain increases from 4% to 8%, the band gap of CGT monolayer decreases due to HVB and LCB move closer to the Fermi level. To understand the origin of such strain dependence of the electronic structure of CGT monolayer, we analyze the PDOS under various biaxial

tensile strains, as illustrated in figure 3(d-f). For the pristine CGT monolayer, the CBM and VBM mainly originate from the Cr *d* orbitals and the Te *p* orbitals, respectively (see figure 3(d)). As tensile strain increases to 8%, the CBM mainly comes from the Cr *d* orbitals and the Te *p* orbitals, while the VBM is always mostly localized at the *p* orbitals of Te atoms (see Figure 3(f)). Note that with strain increases from 0% to 8%, the Cr d orbitals and the Te p orbitals first moves away from the Fermi level and then gets closer to it, which lead to the band gap of CGT monolayer first increases and then decreases. The change trend is consistent with the change of the band structure in CGT monolayer in figure 3(a-c). Furthermore, it can be seen from figure 3(g-i) that the above PDOS analysis is further substantiated by partial charge densities of VBM and CBM in CGT monolayer.

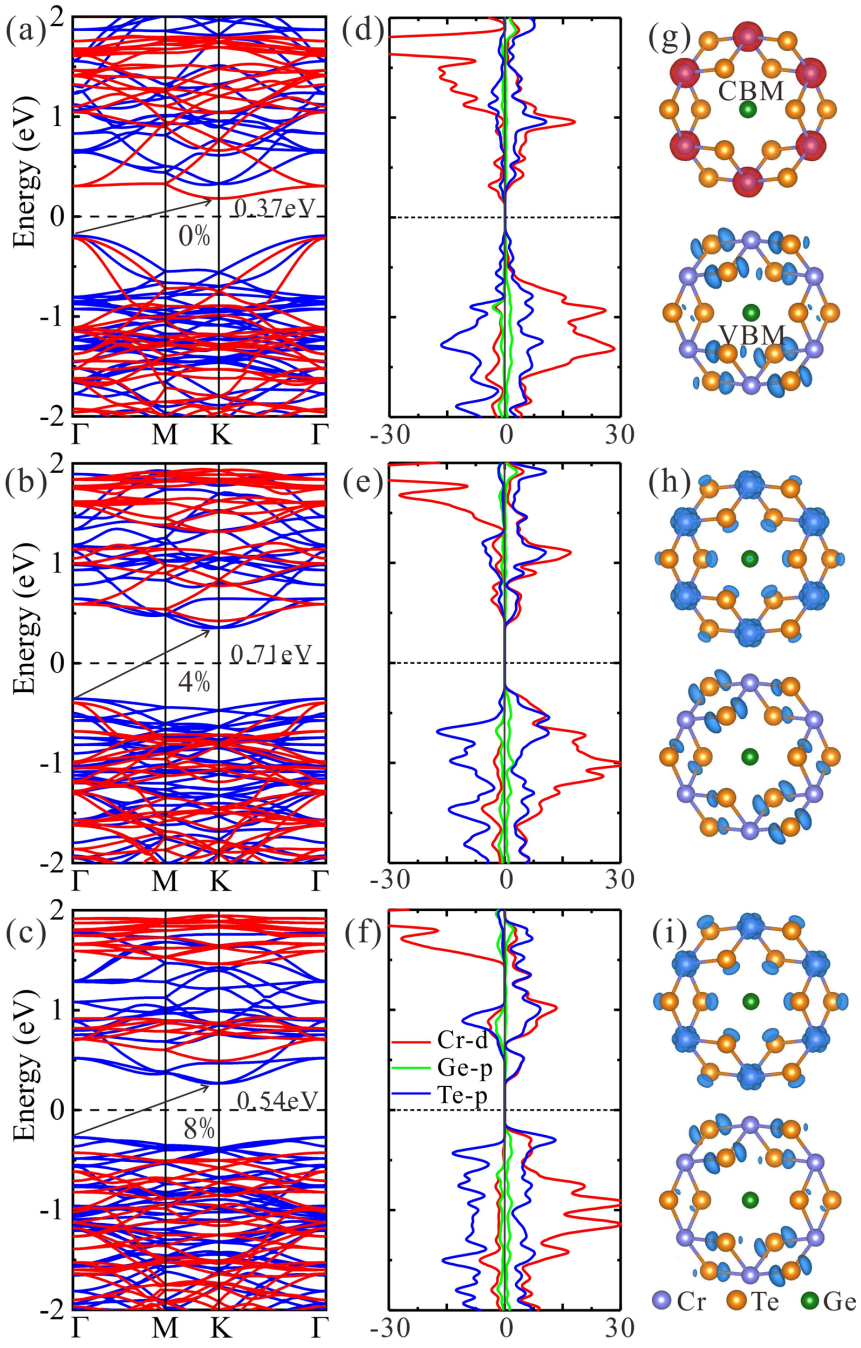

Figure 3. The spin-polarized band structures, PDOS and partial charge densities (the isovalue = 1.5×10^{-3} e/Å^3) of the CGT monolayer under (a, d, g) 0%, (b, e, h) 4%, and (c, f, i) 8% biaxial tensile strain. Blue (red) represent spin-up (spin-down) channels, respectively. The Fermi level is represented by the black dashed line.

In addition to modulation the electronic properties, the biaxial tensile strains also show an interesting response to the magnetic moment of CGT monolayer. The evolution

of atomic magnetic moments in CGT monolayer under different strains are shown in figure 4. Here magnetic moments of Cr, Ge and Te atoms in the CGT were denoted M_{Cr}, M_{Ge} and M_{Te}, respectively. Our calculations demonstrate that magnetic moments increase as strain increases from 0 to 10% in CGT monolayer, as depicted in figure 4. Specifically, the M_{Cr} increases from 3.17 μ_B to 3.40 μ_B with strain increasing from 0% to 10%. On the other hand, the M_{Te} and M_{Ge} increase slightly with increasing biaxial strain in CGT monolayers. This indicates that the spin polarizations in CGT monolayer are mainly contributed by Cr atoms with a small contribution from Ge and Te atoms, which can also be seen in the spin-density distributions. Our results suggest that the magnetic properties in CGT monolayer can be significantly controlled by tensile strain. Assuming that the CGT monolayer can remain stable at strain range up to 10%, the tensile strain can provide a promising route for modulating spin state and magnetic properties.

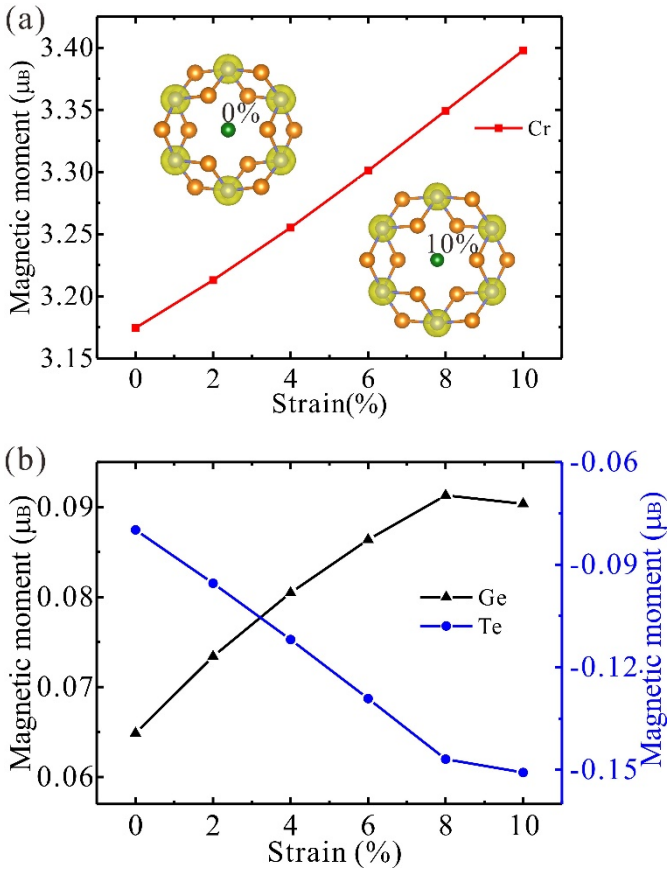

Figure 4. Strain effects on magnetic moment (a) Cr atoms, (b) Ge and Te atoms in the CGT monolayer. The inset schematically shows the spin density distribution of the CGT monolayer under 0% and 10% biaxial strains. The isovalue is set to be 2×10^{-2} e/Å^3.

To better understand in more detail the magnetic moments with strain in CGT monolayer, the bond lengths, charge transfer and PDOS are investigated under a tensile strain. Figure 5(a) shows the bond lengths as a function of a tensile strain. For simplification, the bond lengths of Cr-Te, Ge-Te Ge-Ge and were named $d_{Cr\text{-}Te}$, $d_{Ge\text{-}Te}$ and $d_{Ge\text{-}Ge}$. It is found that the $d_{Cr\text{-}Te}$ and $d_{Ge\text{-}Te}$ increase with strain, while the $d_{Ge\text{-}Ge}$ are almost unchanged. In particular, the $d_{Ge\text{-}Te}$ and $d_{Cr\text{-}Te}$ increase by 4.90% and 3.99% for the CGT monolayer at $\varepsilon = 10\%$ as compared to those for the unstrained case. The change in bond length in the CGT monolayer results in the significant charge transfer shown in figure 5(b). It is noted that as biaxial strain increases, the amount of charge transferred

from the Cr and Te atoms increases. At the same time, the charge transfer is not obvious for Ge atoms. Specifically, Cr atoms lose about 0.25 electron charge, whereas Te (Ge) atoms gain about 0.24 (0.01) electron charge at ε= 10%. Their trend of charge transfer is completely opposite, indicating that charge transfer mainly occurs between Cr and Te atoms. In addition, the shifts of the a and b states of PDOS in figure 5(c) clearly demonstrates that the spin polarization of *d* orbital of the Cr atom near the Fermi level increases with the increase of strain from 2% to 8%, leading to an increase in M_{Cr} from 3.21 μ_B to 3.35 μ_B. Our results suggest that the charge transfer between Cr and Te atoms is very important for the change of magnetic moment with strain in CGT monolayer.

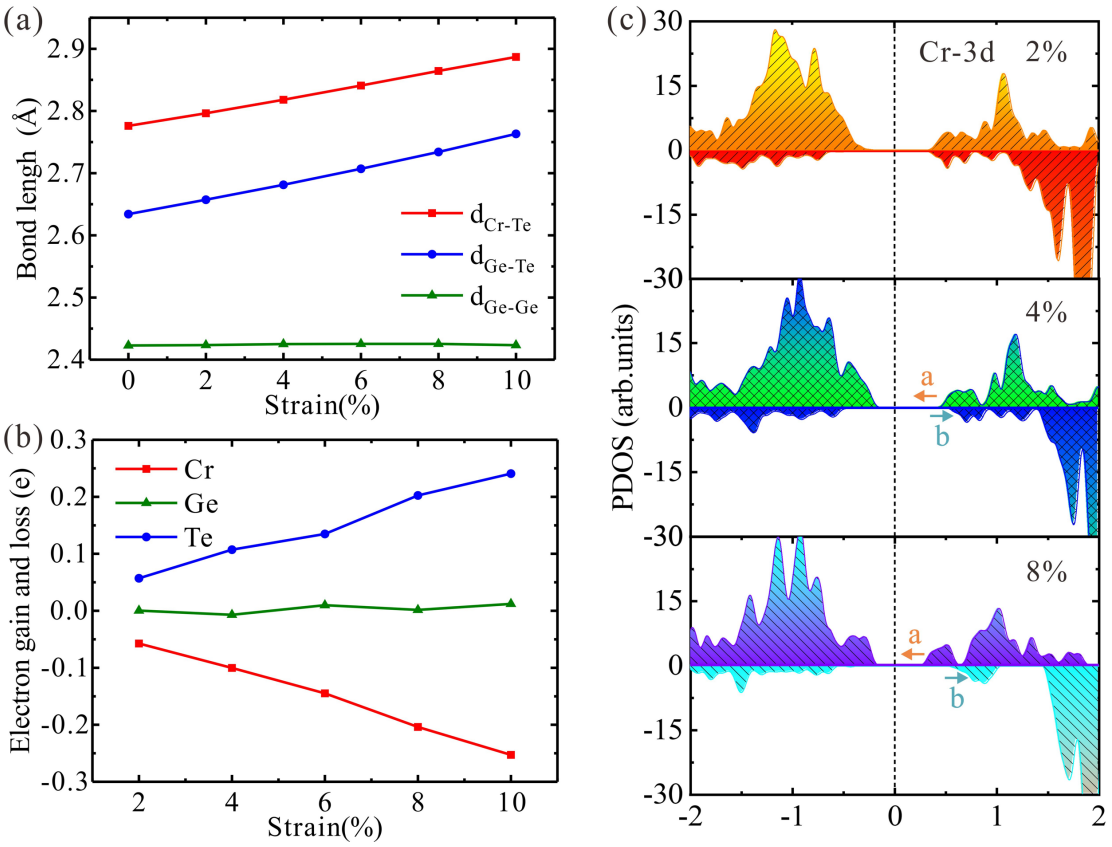

Figure 5. Strain effects on (a) the bonding length, the distance and (b) electron transfer of Cr and Te atoms in the CGT monolayer. (c) The PDOS of Cr atom in CGT monolayer under 2%, 4% and 8% biaxial strain, respectively.

To further understand the impact of biaxial tensile strains on the FM stability of CGT monolayer, the energy difference ΔE ($\Delta E = E_{AFM} - E_{FM}$) at various tensile strains is exhibited in figure 6(a). Our numerical results show that the energy difference presents a monotonous increase as the biaxial tensile increases. Specifically, the energy difference increases by nearly a factor of three with the tensile strain increasing to 10%, as compared to that of the unstretched CGT (from 350 meV to 1025 meV). It can be seen from the increase of energy difference that the stability of the FM state is considerably enhanced, which may be useful for applications of CGT monolayer in spintronic nanodevices.

Moreover, the Curie temperature is one of the critical properties for ferromagnetic materials in nanoelectronics applications. The Curie temperature of CGT monolayer performed by using performing Monte Carlo (MC) simulation based on the 2D Heisenberg Hamiltonian model [49, 50]. $H = -\sum_{i,j} J\, S_i \cdot S_j$ is the Heisenberg spin Hamiltonian, where i and j stand for the nearest Cr atoms, S is the spin operator of Cr site and J is the spin exchange parameter. The exchange energy between FM state and AFM state is calculated by using the following formulas, $E_{FM} = E_0 + E_{ex}$ and $E_{AFM} = E_0 - E_{ex}$ [27], where E_0 represents the non-spin polarized energy of the CGT monolayer per unit cell, E_{FM} and E_{AFM} are the energies of CGT per unit cell in the FM and AFM states. The exchange energy E_{ex} is mapped to the Ising mode to obtain the values of the J parameter (Table S2, Supporting Information), as follows, $J = -E_{ex}/6S^2$. Here, S is the spin of each Cr atom, which is 3/2. The results show that the Curie temperature of the pristine CGT monolayer is estimated to be 58K (figure S4, Supporting Information),

which is consistent with the previous Monte Carlo simulation (57.2K) [49]. However, the T_C of CGT monolayer in the experiment is 22K, which is lower than the value obtained from the Monte Carlo simulation. In order to compare with the experimental data, we corrected it with the following formula, $T_C^{(strain)} = \frac{T_C}{T_C^{MC}} \cdot T_C^{MC(strain)} = 0.379 \cdot T_C^{MC(strain)}$, where T_C and $T_C^{(strain)}$ represent the experimental Curie temperature of CGT and the experimental Curie temperature applied to the strain, respectively. T_C^{MC} and $T_C^{MC(strain)}$ represent the calculated Curie temperature without considering strain and upon applying the strain based on Monte Carlo simulation (Table S2, Supporting Information). The theoretical results in Figure 6a that the tensile strain can effectively modulate the T_C. The change trend of T_C is the same as that of energy difference, which increases as the strain increases. Notably, the Curie temperature can be enhanced by 166% and 191% at 8% and 10% strains, respectively.

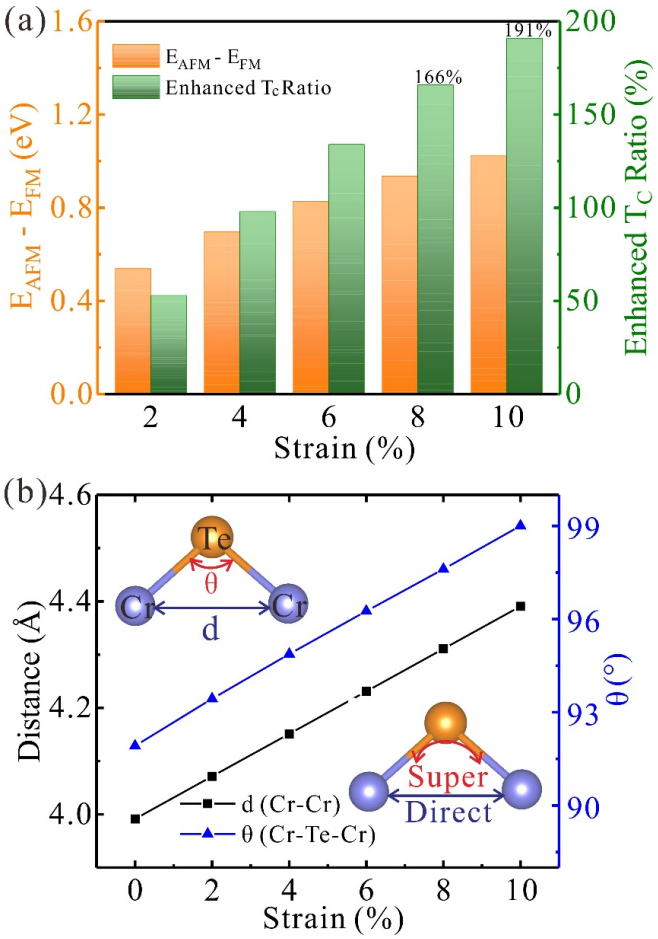

Figure 6. (a) Energy difference between FM and AFM coupling and enhanced Curie temperature of CGT monolayer. (b) Cr atomic distance (*d*) and bond angle Cr-Te-Cr (θ) as a function of strain.

The increase in T_C caused by strain can be explained by Goodenough-Kanamori-Anderson (GKA) rule [51-53]. There is a competition between direct exchange interactions and superexchange interactions in the magnetic ground state of CGT monolayer. We can see that from the bonding structure of figure 6(b), the direct exchange interaction is the direct overlap of the *d* orbitals on the nearest-neighbor Cr atom, which results in the AFM coupling. The superexchange interaction where the d orbitals of Cr and the *p* orbitals of Te atoms overlap, produces FM coupling. The former is mainly determined by the distance between neighboring Cr atoms, while the latter is

mainly influenced by the bond angle Cr-Te-Cr (θ). It can be seen from figure 6(b) that the bond angle (θ) of pristine CGT monolayer is close to 90° (92°), which prefers FM coupling according to the GKA rules. Figure 6(b) shows the distance (d) between Cr atoms and bond angle Cr-Te-Cr (θ) as a function of strain. It can be found that the bond angle θ increases from 92° to 99° as the tensile strain increases, which will lead to the weakness of the superexchange interaction (FM coupling). However, the distance d monotonically increases as the tensile strain. Specifically, the distance d can be increased by more than 10% compared to pristine CGT monolayer at the strain of 10%, which could significantly weaken the direct exchange interaction, i.e., AFM coupling. So, as the tensile strain increases, both the superexchange interaction and the direct exchange interaction become weak. It can be concluded that the enhancement of the ferromagnetism in CGT monolayer under the tensile strain can be attributed to the competition and delicate balance between superexchange interaction and direct exchange interaction.

Conclusions

In summary, the effects of strain on the electronic and magnetic properties of CGT monolayers were systematically studied by means of DFT calculations. Our calculations demonstrated that the band gap of CGT monolayer initially increases finally decreases almost linearly with the increasing tensile strain, which is due to the shift of CBM and VBM. More surprisingly, the Curie temperature of CGT monolayer increased by 191% upon applying 10% strain. The magnetic moment of CGT originates mainly from Cr atoms, and the magnetic moment of Cr atom increases with the increase

of tensile strain. It is shown that the change of magnetic moment is because of the charge transfer caused by the change in bond length. Our results may facilitate experimental work in the field of strain-tunable electromagnetism.

Acknowledgements

This research is supported by the National Natural Science Foundation of China (No.11604047), the Natural Science Foundation of Jiangsu Province (No. BK20160694), Jiangsu Planned Projects for Postdoctoral Research Funds (No. 2019K010A), the Priority Academic Program Development of Jiangsu Higher Education Institutions (PAPD), and in USA by NASA (Grant Number 80NSSC19M0236) and NSF Center for the Advancement of Wearable Technologies (Grant 1849243). AVK acknowledges funding from the German Research Foundation (DFG), project KR 48661/2. We are grateful to the High Performance Computing Center of Nanjing Tech University for supporting the computational resources.

References

[1] Novoselov K S, Geim A K, Morozov S V, Jiang D, Zhang Y, Dubonos S V, Grigorieva I V and Firsov A A 2004 *Science* 306 666-9

[2] Sun J Y, Lu C, Song Y Z, Ji Q Q, Song X J, Li Q C, Zhang Y F, Zhang L, Kong J and Liu Z F 2018 *Chemical Society Reviews* 47 4242-57

[3] Hu X H, Wang Y F, Shen X D, Krasheninnikov A V, Sun L T and Chen Z F 2018 *2d Materials* 5 10

[4] Kou L Z, Ma Y D, Sun Z Q, Heine T and Chen C F 2017 *Journal of Physical Chemistry Letters* 8 1905-19

[5] Ma Y D, Jing Y and Heine T 2017 *2d Materials* 4 6

[6] Wang Y, Li Y F and Chen Z F 2020 *Accounts of Chemical Research* 53 887-95

[7] Wu Q S, Xu W W, Lin D D, Wang J L and Zeng X C 2019 *Journal of Physical Chemistry Letters* 10 3773

[8] Liu H L, Yang T, Chen J H, Chen H W, Guo H, Saito R, Li M Y and Li L J 2020 *Scientific reports* 10 15282

[9] Wang J Z, Yang T, Zhang Z D and Yang L 2018 *Applied Physics Letters* 112 5.

[10] Yazyev O V and Helm L 2007 *Physical Review B* 75 5

[11] Avsar A, Ciarrocchi A, Pizzochero M, Unuchek D, Yazyev O V and Kis A 2019 *Nature Nanotechnology* 14 674

[12] Karthikeyan J, Komsa H P, Batzill M and Krasheninnikov A V 2019 *Nano Letter* 19 4581-7

[13] Hu X, Zhang W, Sun L and Krasheninnikov A V 2012 *Physical Review B* 86 195418

[14] Hu X, Wan N, Sun L and Krasheninnikov A V 2014 *The Journal of Physical Chemistry C* 118 16133–9

[15] Sui X, Si C, Shao B, Zou X, Wu J, Gu B-L and Duan W 2015 *The Journal of Physical Chemistry C* 119 10059-63

[16] Ai W, Kou L, Hu X, Wang Y, Krasheninnikov A V, Sun L and Shen X 2019 *Journal of Physics: Condensed Matter* 31 445301

[17] Huang B, Clark G, Navarro-Moratalla E, Klein D R, Cheng R, Seyler K L, Zhong D, Schmidgall E, McGuire M A, Cobden D H, Yao W, Xiao D, Jarillo-Herrero P and

Xu X 2017 *Nature* 546 270

[18] Gong C, Li L, Li Z L, Ji H W, Stern A, Xia Y, Cao T, Bao W, Wang C Z, Wang Y A, Qiu Z Q, Cava R J, Louie S G, Xia J and Zhang X 2017 *Nature* 546 265

[19] Deng Y J, Yu Y J, Song Y C, Zhang J Z, Wang N Z, Sun Z Y, Yi Y F, Wu Y Z, Wu S W, Zhu J Y, Wang J, Chen X H and Zhang Y B 2018 *Nature* 563 94

[20] Pizzochero M 2020 *Journal of Physics D-Applied Physics* 53 244003

[21] Fei Z Y, Huang B, Malinowski P, Wang W B, Song T C, Sanchez J, Yao W, Xiao D, Zhu X Y, May A F, Wu W D, Cobden D H, Chu J H and Xu X D 2018 *Nature Materials* 17 778

[22] Fang Y M, Wu S Q, Zhu Z Z and Guo G Y 2018 *Physical Review B* 98 13

[23] Ostwal V, Shen T T and Appenzeller J 2020 *Advanced Materials* 32 7

[24] Shang J, Tang X, Tan X, Du A J, Liao T, Smith S C, Gu Y T, Li C and Kou L Z 2020 *ACS Applied Nano Materials* 3 1282-8

[25] Sun Y, Tong W and Luo X 2019 *Physical Chemistry Chemical Physics* 21 25220-5

[26] Xu C S, Feng J S, Xiang H J and Bellaiche L 2018 *npj Computational Materials* 4 6

[27] He J, Ding G, Zhong C, Li S, Li D and Zhang G 2019 *Journal of Materials Chemistry C* 7 5084-93

[28] Song C S, Xiao W, Li L, Lu Y, Jiang P H, Li C R, Chen A X and Zhong Z C 2019 *Physical Review B* 99 214435

[29] Song C, Liu X, Wu X, Wang J, Pan J, Zhao T, Li C and Wang J 2019 *Journal of*

Applied Physics 126 105111

[30] Liu L, Kou L, Wang Y, Lu C and Hu X 2020 *Nanotechnology* 31 455702

[31] Johari P and Shenoy V B 2012 *Acs Nano* 6 5449-56

[32] Zhang Z, Zhao Y and Ouyang G 2017 *The Journal of Physical Chemistry C* 121 19296-304

[33] Webster L and Yan J A 2018 *Physical Review B* 98 144411

[34] Tang X, Sun W, Gu Y, Lu C, Kou L and Chen C 2019 *Physical Review B* 99 045445

[25] Ma Y, Dai Y, Guo M, Niu C, Yu L and Huang B 2011 *Nanoscale* 3 2301-6

[36] Ma Y, Dai Y, Guo M, Niu C, Zhu Y and Huang B 2012 *ACS Nano* 6 1695-701

[37] Ma F X, Gao G P, Jiao Y L, Gu Y T, Bilic A, Zhang H J, Chen Z F and Du A J 2016 *Nanoscale* 8 4969-75

[38] Dai Z H, Liu L Q and Zhang Z 2019 *Advanced Materials* 31 11

[39] Peng Z W, Chen X L, Fan Y L, Srolovitz D J and Lei D Y 2020 *Light-Science & Applications* 9 25

[40] Zhou M, Chen X, Li M and Du A 2017 *Journal of Materials Chemistry C* 5 1247-54

[41] Kresse G and Furthmüller J 1996 *Physical Review B* 54 11169-86

[42] Kresse G and Furthmüller J 1996 *Computational Materials Science* 6 15-50

[43] Blöchl P E 1994 *Phys. Rev. B* 50 17953-79

[44] Kresse G and Joubert D 1999 *Physical Review B* 59 1758-75

[45] Perdew J P, Burke K and Ernzerhof M 1996 *Physical Review Letters* 77 3865-8

[46] Heyd J, Scuseria G E, Ernzerhof M 2003 *The Journal of Chemical Physics* 118

8207-15

[47] Wang K Y, Hu T, Jia F H, Zhao G D, Liu Y Y, Solovyev I V, Pyatakov A P, Zvezdin A K and Ren W 2019 *Applied Physics Letters* 114 5

[48] Qi J, Qian X, Qi L, Feng J, Shi D and Li J 2012 *Nano Letter* 12 1224-8

[49] Li X and Yang J 2014 *Journal of Materials Chemistry C* 2 7071-6

[50] Kulish V V and Huang W 2017 *Journal of Materials Chemistry C* 5 8734-41

[51] Goodenough J B 1955 *Physical Review* 100 564-73

[52] Anderson P W 1959 *Physical Review* 115 2-13

[53] Kanamori J 1960 *Journal of Applied Physics* 31 S14-S23